Domain growth in a one-dimensional diffusive lattice gas with short-range attraction

Donald J. Jacobs
Institute for Theoretical Physics, Princetonplein 5, P.O. Box 80006, 3508 TA Utrecht, The Netherlands

Andrew J. Masters
Department of Chemistry, Manchester University, Manchester M13 9PL, United Kingdom
(Received 28 October 1993)

A one-dimensional diffusive lattice gas with an attractive interaction between particles a distance r apart is introduced which violates detailed balance. For interactions of sufficient strength and range, there exists a density regime within which a state of uniform density is not a stable, equilibrium solution. Via computer simulation, we studied the time evolution of a system initially prepared in such an unstable, uniform state. Domains of high and low density were observed to form and these subsequently grew. The typical length of a domain at time t, $R(t)$, was inferred to asymptotically obey the growth law $R(t) \sim t^{1/3}$, the same result as found in phase-ordering dynamics for higher-dimensional systems with a conserved, scalar order parameter. The structure factor and density-density correlation function were found to scale with $R(t)$, but the forms of the scaling functions were density dependent.

PACS number(s): 02.50.−r, 64.60.Ht, 05.20.Dd, 05.70.Ln

I. INTRODUCTION

The basic idea of a lattice gas is to simulate the evolution of a system of classical particles by keeping track of each particle's trajectory and accounting for collisions when they occur. The lattice gas is similar to molecular dynamics in this sense except that the particles are confined to move on a lattice with only a small number of allowed discrete velocities. The dynamics of a lattice gas is broken up into a collision step and a propagation step. The collision step is generally a stochastic process determining how a set of indistinguishable particles at a node change from their incoming velocity channels to a set of outgoing velocity channels. The propagation step is a free streaming of the particles to a nearest-neighbor node in the direction of the outgoing velocity channel. Each of these steps is a parallel process (occurring at each node simultaneously) and the succession of both steps together form one discrete time increment. It is well known that a lattice gas can model nonequilibrium fluids reasonably well [1].

With a rather different focus, a diffusive lattice gas would apply either to a system of particles at a coarse-grained level of description or to particles diffusing in a solid matrix. The velocity variable would not be expected to play an important role since any propagation mode would be damped. However, in the spirit of the Boghosian-Levermore lattice gas [2], it proves convenient to keep the lattice-gas framework where the velocity channels define preferred directions for the particles to move and a Fermi exclusion rule is automatically enforced.

The model we introduce does not generally satisfy detailed balance, which implies $W_{BA}P_A \neq W_{AB}P_B$ with no summation on repeated indices. Here P_X is the stationary probability of finding the system in microstate X and W_{XY} is the probability for the system to change from microstate Y to X where X and Y may equal A or B. This model serves as another example of a general class of lattice-gas automata that exhibits interesting behavior when detailed balance is violated. It has been observed [2–5] that a lack of detailed balance in lattice-gas models may cause instabilities in a uniform state and possibly lead to phase separation. Detailed balance can be broken in a number of different ways which may stem from internode collision rules [4], intranode collision rules [5], or simply applying an external bias [2,3] (e.g., possibly due to a gravitational field).

The diffusive lattice gas is useful to study the kinetics of a first-order phase transition of a binary system where mass transport is diffusion controlled. More specifically, we are interested in the long-time coarsening of a system below the critical point within the coexistence region which initially was in a uniform state. There has already been substantial numerical simulation of the ripening process (late-time coarsening of domains) using the spin-exchange kinetic Ising model [6] and the continuum Langevin model with a conserved scalar order parameter [7] in two dimensions. The diffusive lattice gas is another alternative for numerical simulations, and can be studied theoretically from a kinetic approach usually within a mean-field approximation using a corresponding lattice Boltzmann equation [8].

The dynamical-scaling assumption [9] is expected to hold for the ripening process of the diffusive lattice gas (as for the other models) provided that the average domain size $R(t)$ gives the only relevant characteristic length scale in the problem. However, the domain growth law $R(t) \sim t^a$ may be different from previously studied models, since the growth exponent depends on the micro-

scopic mechanism of mass transport and dimensionality. We study a one-dimensional system which has the advantage of being easier to work with both theoretically and numerically than systems of higher dimension. For instance, a surface-curvature mechanism cannot exist and this means that domain growth will be driven by fluctuations (thermal noise) and from weakly overlapping exponential tails in the concentration profile between neighboring domains [9].

When growth is driven by fluctuations, a scaling argument for d dimensions given by Binder and Stauffer [10] predicts growth exponents of $1/(3+d)$ and $1/(2+d)$ for the surface and bulk diffusion mechanisms, respectively. Restricting our discussion to one dimension, we therefore might expect a growth exponent of $1/4$ or $1/3$ as Furukawa [9] summarizes. On the other hand, without sufficient fluctuations, a logarithmic growth due to the weak overlap of the exponential tails may be expected.

The domain growth for either the "surface" or bulk diffusion mechanism is a result of domains diffusing into one another. The growth law depends on the way the diffusion coefficient of a domain D^* scales with its length l. Now D^* depends on how the domain's center of mass shifts as minority carriers diffuse across its length.

The surface diffusion mechanism applies when each domain only has one minority carrier traveling within it. A mean time t_d for the displacement of the domain's center of mass to change one unit ($\Delta x = \pm 1$) is just the diffusion time for the minority carrier to cross the domain (which scales as $\sim l^2$). Since the diffusion coefficient for a domain of length l is given by $D^* = \langle \Delta x^2 \rangle / t_d$, it follows that $D^* \sim 1/l^2$. A bulk diffusion mechanism applies when the number of minority carriers is proportional to the domain length. Then within the time t_d the mean squared displacement of the domain's center of mass is determined by its mean number of carriers which scales as $\langle \Delta x^2 \rangle \sim l$, and this leads to the relation $D^* \sim 1/l$.

The plan of the paper is as follows. We introduce our model in Sec. II and show under what conditions a state of uniform density becomes unstable. Numerical simulation data are presented in Secs. III and IV for a simplifying choice of parameters for which a particle-hole duality exists. The late-time coarsening is analyzed in Sec. III where the domain growth mechanism is described by an evaporation and condensation process. The data suggest an asymptotic growth of $t^{1/3}$ for which we give a simple supporting argument. From the structure factor and the density-density correlation function we show in Sec. IV that dynamical scaling holds at late times for the half filled lattice. Scaling is found for a $1/5$ filled lattice at times before the domain growth starts to exhibit a simple power-law dependence. Finally, we conclude in Sec. V.

II. MODEL

We construct a diffusive lattice-gas model on a one-dimensional lattice with periodic boundary conditions. Each node contains two channels. We denote the occupation numbers for the right- and left-directed channels at node x, and time t, by $n_1(x,t)$ and $n_2(x,t)$, respectively. The occupation number $n_j(x,t)$ is equal to 0 or 1 only and the set of all occupation numbers $\{n_j(x,t)\}$ defines the state of the system at time t. Note that the explicit time dependence will often be suppressed in the equations that follow.

Let us define the state of a particular node as $[n_2, n_1]$, which can take on four possible states. The collision rule for an empty node is that it remains empty, so $[0,0] \rightarrow [0,0]$ with probability one. Similarly, $[1,1] \rightarrow [1,1]$ with probability one. For a single particle on a node, a back-step probability of p_b is assigned for the particle to change channels with probability $1-p_b$ for no change. A *nonlocal* interaction between particles is built into the collision step by having the back-step probability p_b be dependent on the configuration of nodes in a small neighborhood. In addition to the node of interest $[n_2(x), n_1(x)]$, we choose the configuration to include the two receding channels (directed away from node x), one located at $x-r$ and the other at $x+r$ [i.e., $n_2(x-r)$ and $n_1(x+r)$]. We could equally well have chosen two approaching channels (inwardly directed toward node x). Other interactions could be considered by including both receding and approaching channels such as using the total occupation number at a node. Our choice for determining p_b is much simpler than using the total occupation number at a node, yet allows us to model a "square-well potential."

The rules for all possible configurations are summarized in Table I for a single particle initially in a right channel where p_b is conditional on $n_2(x-r)$, $[n_2(x), n_1(x)]$, and $n_1(x+r)$. By inversion symmetry, the four probabilities listed in Table I completely specify the general model without an external bias. In the limit of vanishing density, the probability p_1 determines the self-diffusion coefficient of the particles. In the opposite limit (i.e., a full lattice), p_4 determines the self-diffusion coefficient of the holes. When $p_1 = p_4$ the model has an additional symmetry of particle-hole duality. For an attractive interaction, one can set $p_2 < 1/2$ and $p_3 > 1/2$ and vice versa for a repulsive interaction. Clearly this collision rule gives us a model which is quite flexible, perhaps too much in the sense that we will soon limit ourselves to a special case.

The collision step being a stochastic process is implemented by introducing a set of four random variables $\{\alpha_m\}$ where α_m equal 0 or 1 with probability

$$p(\alpha_m) = p_m \delta_{1,\alpha_m} + (1-p_m)\delta_{0,\alpha_m} , \qquad (1)$$

where $\langle \alpha_m \rangle = p_m$. The set of random variables $\{\alpha_m\}$ (at all nodes) are independent and uncorrelated. De-

TABLE I. The collision rules for a single particle at node x in the right channel, where p_b is the probability that the post-collision state will be $[1,0]$.

p_b	$n_2(x-r)$	$[n_2(x), n_1(x)]$	$n_1(x+r)$
p_1	0	[0,1]	0
p_2	0	[0,1]	1
p_3	1	[0,1]	0
p_4	1	[0,1]	1

noting the outcome of a collision at a node as $[n_2', n_1']$, the collision step can be efficiently performed on a *scalar* computer by first assuming that the post-collision state $[n_2', n_1']$ is equal to the precollision state $[n_2, n_1]$. Only when one particle is at the node does the conditional probability for a backstep need to be looked up by checking the channels at $x \pm r$. If a test random number is drawn above the conditional probability p_b, the assumed post-collision state is correct; otherwise $[n_2' = n_1, n_1' = n_2]$ will be the post-collision state. This process is carried out over the entire lattice in parallel because the final outcome at a node depends only on the *pre-collision* occupation numbers.

We next perform the propagation step given as $n_j(x + c_j, t+1) = n_j'(x,t)$, where $c_1 = 1$, $c_2 = -1$, and n_j' is a post-collision occupation number. Combining the collision and propagation steps together yields the stochastic dynamical equations of evolution,

$$\begin{aligned} n_j(x+c_j,t+1) = n_j &+ (n_{j+1}-n_j)[\alpha_1 \bar{n}_2(x-r)\bar{n}_1(x+r) + \alpha_4 n_2(x-r)n_1(x+r)] \\ &+ n_{j+1}\bar{n}_j[\alpha_2 n_{j+1}(x+rc_{j+1})\bar{n}_j(x+rc_j) + \alpha_3 \bar{n}_{j+1}(x+rc_{j+1})n_j(x+rc_j)] \\ &- \bar{n}_{j+1}n_j[\alpha_3 n_{j+1}(x+rc_{j+1})\bar{n}_j(x+rc_j) + \alpha_2 \bar{n}_{j+1}(x+rc_{j+1})n_j(x+rc_j)] , \end{aligned} \tag{2}$$

where $\bar{n}_j = 1 - n_j$ and j is taken to be cyclic. If not explicitly expressed, the arguments of the variables on the right hand side of Eq. (2) are understood to be at node x and time t. We note that by allowing r to be negative, a model with the backstep probability being conditional on the approaching channels at $x \pm r$ can be studied as well. Inspection of Eq. (2) shows that mass is conserved and that the occupation numbers retain the Fermi exclusion property. Momentum is conserved neither locally nor globally.

There are a couple of less obvious properties of the dynamical equation of evolution worthy of note. Since the lattice is bipartite and the particles are propagated to a nearest-neighbor node every time step, there is a conserved staggered density [8]. For example, the particles initially on sublattice A (all even x) can always be found on sublattice A at even time steps and on sublattice B (all odd x) at odd time steps. More importantly, the two sublattices form uncoupled systems if r is even (and, because of the periodic boundary conditions, provided the lattice is of even length). With r odd, interactions are only between particles that are on different sublattices. In either case the model has a few properties that are physically unrealistic. However, for r even, both pathologies are absent when each sublattice is considered separately, and new coordinates (x', t') are introduced, where $x' = x/2$ and $t' = t/2$ ($r' = r/2$ may be even or odd). Note that two collision steps are performed between two different pair of channels per unit of time. The evolution of each subsystem is found to be basically the same as that of the full system with r odd. Therefore we suspect the model pathologies do not play any crucial role when r is odd.

The question we now address is whether a state of uniform density is stable to small density fluctuations. We begin with the lattice Boltzmann equation corresponding to the stochastic evolution of Eq. (2). The lattice Boltzmann equation is a mean-field approximation that neglects correlations in the occupation numbers of different states. The time-dependent probability for the state of the system (over an ensemble of all realizations for the collisions and initial conditions) is assumed to be a product measure given by

$$\mathrm{Prob}[\{n_j(x)\}] = \prod_{x=1}^{N}\prod_{j=1}^{2}[f_j(x)]^{n_j(x)}[\bar{f}_j(x)]^{\bar{n}_j(x)} , \tag{3}$$

where $\bar{f}_j(x) = 1 - f_j(x)$ and $f_j(x)$ is the probability for $n_j(x) = 1$ at time t. The resulting lattice Boltzmann equation is thus given by Eq. (2) with the replacements $n_j \to f_j$ and $\alpha_m \to p_m$.

The lattice Boltzmann equation is linearized using $f_j(x) = f_0 + \delta f_j(x)$, where f_0 is the reduced average concentration of particles and $\delta f_j(x)$ is assumed arbitrarily small so that we can neglect terms of order $O(\delta f^2)$. Upon taking the Fourier transform of the linearized Boltzmann equation, we can express the resulting equation in the usual form [8]

$$[(e^{z_\lambda(k)+ikc_j} - 1)\delta_{jl} - \Omega_{jl}(k)]\psi_l^\lambda = 0 , \tag{4}$$

where the form of the Fourier component of $\delta f_j(x)$ is taken as $\psi_j(k)\exp[z(k)t]$ and λ labels the eigenmodes. The matrix elements of the linearized collision operator $\hat{\Omega}$ work out to be $\Omega_{22}(k) = \Omega_{11}^*(k)$, $\Omega_{21}(k) = -\Omega_{11}(k)$, $\Omega_{12}(k) = -\Omega_{11}^*(k)$, and

$$\Omega_{11}(k) = -\{p_1\bar{f}_0^2 + [p_2 + p_3 + (p_2 - p_3)e^{ikr}]\bar{f}_0 f_0 + p_4 f_0^2\}. \tag{5}$$

Here $\bar{f}_0 = 1 - f_0$ and r is the range of interaction.

The eigenmodes $\psi^\lambda(k)$ of the linearized Boltzmann equation are stable when $\mathrm{Re}[z_\lambda(k)] < 0$, conserved when $\mathrm{Re}[z_\lambda(k)] = 0$, and unstable when $\mathrm{Re}[z_\lambda(k)] > 0$. For attractive interactions it is possible to find diffusive modes that are unstable for $kr \ll 1$ as well as modes that are unstable at larger wave numbers. There are no unstable or conserved propagating modes in the limit $kr \ll 1$. Although we have obtained the entire spectrum for the linearized collision operator for this model, we will concentrate on the stability of the diffusive mode in the long-wavelength limit. In doing so, we obtain the collective diffusion coefficient where a local diffusion constant only exists on length scales much greater than the range of interaction.

The eigenvalue of the diffusive mode $z_D(k)$ is of the

form $-Dk^2$ in the $k \to 0$ limit where D is the diffusion constant. We find for the general model

$$D = (1 - p_{\text{eff}})/2p_{\text{eff}} + \Delta p \bar{f}_0 f_0 r/p_{\text{eff}} , \quad (6)$$

where $\Delta p = p_2 - p_3$ and

$$p_{\text{eff}} = -\Omega_{11}(0) = p_1 \bar{f}_0^2 + 2p_2 \bar{f}_0 f_0 + p_4 f_0^2 . \quad (7)$$

The asymmetry of Eq. (7) having $2p_2$ instead of $(p_2 + p_3)$ with the weight $\bar{f}_0 f_0$ can be traced back to Eq. (5) where the term $(p_2 - p_3)e^{ikr}$ corresponds to a *nonlocal* transfer of probability due to the interaction at $\pm r$ distance. The interaction strength is determined by Δp, where the sign determines whether the interaction is attractive ($\Delta p < 0$) or repulsive ($\Delta p > 0$). For $\Delta p = 0$, the diffusion coefficient is that of an independent persistent random walker with a backstep probability given by p_{eff}.

The sign of the diffusion coefficient in the linear analysis determines the stability of the diffusive mode. We see that the diffusive mode in the $k \to 0$ limit is stable when $\Delta p > 0$, but for $\Delta p < 0$, it becomes unstable for sufficiently large r. The mean-field approximation in arriving at the lattice Boltzmann equation must be justified of course. For example, the range r cannot become arbitrary large, since it must remain on microscopic length scales.

We now consider in this paper the special case where $p_1 = p_2 = p_4 = p$ and $p_3 = 1 - p$, which has a simple interpretation. A single particle at a node will be directed up a concentration gradient (when one exists) because of the attractive interaction, and then with probability p may change direction (channels) because of the local influence of the medium. From Table I, only the configuration in the third row has a concentration gradient that causes the particle at node x to enter the left channel where it then has probability p to change channels. Note that the holes have the same dynamics as the particles.

For this special case, the diffusion coefficient is given by

$$D = (1 - p)/2p + (2p - 1)\bar{f}_0 f_0 r/p , \quad (8)$$

which is parabolic in the reduced average particle concentration with an extremum at the half filled lattice. The first term is a bare diffusivity while the second term accounts for the interparticle interactions. We only consider $p \leq 1/2$ since we are interested in attractive interactions. A critical probability p_c is defined for which the minimum value of the diffusion coefficient at a half filled lattice is zero. For $p_c \leq p \leq 1/2$ all modes are stable and the uniform density profile is expected to be stable. We find that $p_c = 0$ for $r \leq 2$ and $p_c = (r - 2)/(2r - 2)$ for $r \geq 3$. For $p < p_c$ there will be a range of reduced densities $f_c(p) \leq f_0 \leq 1 - f_c(p)$ for which the diffusion coefficient is negative. We therefore define a spinodal such that everywhere within the spinodal line the system is unstable to infinitesimal long-wavelength density fluctuations. The lower branch of the spinodal line is given by

$$f_c(p) = \frac{1}{2} - \frac{1}{2}\sqrt{1 - \frac{2(1-p)}{r(1-2p)}} . \quad (9)$$

The spinodal line is contained within the coexistence region and cannot predict the average density for which the system will remain with a uniform density profile. For this, the binodal line is needed which can be determined from the stationary solution to the full nonlinear lattice Boltzmann equation. In a similar spirit to the work of Gobron [11], but with less rigor, an approximate stationary solution has been found for the restricted model. These and related results will be published elsewhere. We only wish to point out that a system with an average density lying outside the spinodal region and for $p < p_c$ may still possibly phase separate. The initial forming of domains will take a much longer time because only the nonlinear terms are responsible, and therefore the system is "metastable." The quotes are used because the distinction between the metastable and spinodal regions is not very sharp for short-range interactions.

III. DOMAIN GROWTH

In Sec. II we introduced a diffusive lattice-gas model which is unstable to long-wavelength density fluctuations within the calculated spinodal region. However, knowing that a uniform density profile is unstable does not imply that the system will coarsen toward a phase-separated state. It is possible that while the stationary solution of the nonlinear Boltzmann equation predicts a phase-separated state, microscopic fluctuations could destroy the mean-field prediction. The goals of this section are to demonstrate that this model can support well defined domains, to understand the growth mechanism, to determine the growth law, and to give a simple picture for the ripening process which is consistent with these findings.

The questions of whether well defined domains form, and if so, whether they coarsen are best answered by considering a simulation and by looking at the evolution of the density profile. We show in Fig. 1 several snapshots of the density profile during a simulation run for a small system at an approximately half filled lattice. Since the allowed number of particles per node are 0, 1, and 2, the concept of a density is meaningless without some sort of coarse graining. In Fig. 1 we have smoothed the data according to a binomial weight of the form

$$\rho(x,t) = \frac{1}{2^M}\sum_{m=0}^{M}[n_2(x - M/2 + m, t) + n_1(x - M/2 + m, t)]\frac{M!}{(M-m)!m!} , \quad (10)$$

where $M = 10$, but M could be set to any even integer. A uniform weight over the same interval gave a smoother profile on the whole, but the binomial weight has more resolution to view the fluctuations which are our main interest.

All of the simulations in this paper start with an initial state that is generated by introducing a particle into each channel with a probability f_0 (the reduced average density). Since we do not enforce a precise number of

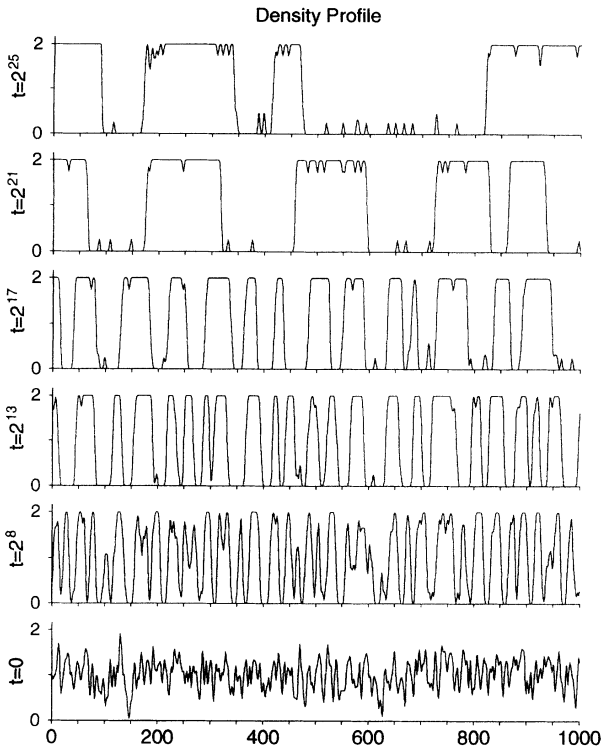

FIG. 1. Several snapshots of the density profile for one realization with $r = 5$ and $p = 0.25$ on a lattice of 1024 sites containing 1040 particles. Only a 1000 site section is shown.

particles, the actual average density ρ_0 varies slightly between realizations. The initial uniform density profile is shown at the bottom of Fig. 1 and it gives an idea of the scale at which the fluctuations may be observed. As time passes, well defined domains are seen to form and subsequently to grow. Low- and high-density domains contain particles and holes, respectively, which form a minority density. Most of the peaks and antipeaks which appear in the last three frames correspond to single minority carriers, and these are sufficiently far apart that they can be regarded as noninteracting.

The microscopic dynamics can be idealized given the fact that sharp interfaces form between domains and given the assumption that the minority carriers are independent. Holes within the interaction range r from an interface, on the side of high density, have an approximate drift velocity of $1 - 2p$ toward the low-density domain. Similarly, particles have an approximate drift velocity of $1 - 2p$ toward the high-density domain. A sharp step in the density profile is responsible for this homing bias which is on both sides of each domain. With the Fermi exclusion keeping the domains from collapsing, the interface is very stable and self-supporting because of this constant squeezing pressure. Occasionally holes (particles) will escape the biased region into the high- (low-) density domain which is like an activated process.

From Fig. 1 it is not clear *how* the domains coarsen. It appears that within each domain there is a very low density of diffusing minority carriers. Figure 1 suggests that the number of minority carriers on average is proportional to the domain length, leading one to speculate a bulk diffusion mechanism. However, when there is particle-hole duality and at a half filled lattice, both the low- and high-density domains will have statistically identical dynamics. By geometry and mass conservation it is impossible for all domains to remain roughly the same size as they diffuse. Obviously some domains must evaporate away. Therefore the dynamics is best described in terms of an evaporation and condensation mechanism.

Consider the ripening process beginning with carriers evaporating from two parent domains separated by a domain of opposite phase. The rate of evaporation is *independent* of the parent domain size (except for domains of length $l \leq r$ as they break up). For mass transport to occur, a minority carrier starting from the left (right) parent domain must condense on the right (left) parent domain. Therefore the gain or loss in size of either parent domain depends on *fluctuations* in this totally symmetrical situation. In time some domains will totally evaporate away, given room for its two neighboring domains of opposite phase to join. We note that without particle-hole duality, it is possible, for example, to make the average *minority density* of particles much less than that of holes. Then the high-density phase cannot evaporate as easily because low-density domains are not as frequently allowing particles to pass. Therefore the high-density domains will have greater mobility and will appear to grow by diffusing into each other. We conclude that the evaporation and condensation mechanism describes the ripening process fully and in a unified way.

The domain growth is investigated for an interaction range $r = 5$ with $p = 0.25$ at several average densities $\langle\rho\rangle = \{1.1, 1.0, 0.8, 0.7, 0.4\}$ as well as $p = 0.01$ at the average densities $\langle\rho\rangle = \{1.0, 0.4\}$. The angular brackets $\langle\,\rangle$ denote an average over an ensemble of all realizations (including initial conditions) so that $\langle\rho\rangle = 2f_0$. For $r = 5$, $p_c = 0.375$ and each average density considered lies within the spinodal. We determine the characteristic length of the system using the first zero in the equal time density-density correlation function. The density-density correlation function is given by

$$g(x,t) = \frac{1}{N}\sum_{y=1}^{N}\langle \delta n(y+x,t)\delta n(y,t)\rangle \,, \tag{11}$$

where $\delta n(x,t) = n_2(x,t) + n_1(x,t) - 2f_0$. Note that with periodic boundary conditions the summation in Eq. (11) is modified to $(y+x)$ mod$N$. To obtain this function, we first calculate the structure factor which is given by

$$S(k,t) = \frac{1}{N}\langle \mid \delta\tilde{n}(k,t) \mid^2 \rangle \,, \tag{12}$$

where $\delta\tilde{n}(k)$ is the Fourier transform of $\delta n(x)$. Then $g(x,t)$ is obtained from $S(k,t)$ by inverse Fourier transforming. Both calculations are very efficient with the use of the fast Fourier transform [12].

The average domain size determines the characteristic length scale of the system. Other ways of characterizing the domain size include using the density-density correlation function or the structure factor. The first zero of the

density-density correlation function is used for this purpose because it is efficient to calculate and is a quantity that self-averages (see Amar *et al.* [6]). The first zero $R(t)$ of the function $g(x,t)$ is therefore more accurate than the inverse of the wave number at which $S(k_m,t)$ is a maximum since k_m does not self-average. An alternative would be to use the inverse of the average wave number using $S(k,t)$ as a weight function.

As might be expected from the results of simulations on other models, the domain growth will not be a simple power law. The power law is only approached asymptotically. The time that is needed to unambiguously determine the growth exponent is unfortunately longer than we can reach by simulations and so we need to fit also subleading asymptotic terms. We have managed to go as high as 2^{25} time steps for a system size of 2^{14} sites. To go further in time steps would require an even larger system to avoid boundary effects. Most of our data are for a system size of 2^{16} sites running to 2^{20} time steps. A long run takes about 100 h of CPU time on a Sparc workstation.

We believe that our results are free from any substantial finite-size effects. We found good agreement at long times between the density-density correlation functions calculated for system sizes between 2^{10} and 2^{16} sites. Once assured that a system of size $N_0 = 2^{10}$ was yielding the same results as the larger systems up to a time t_0, we always made sure that we ran the simulation for a system of size N up to a maximum time less than $t_0 N^2/N_0^2$. Therefore a tagged particle is extremely unlikely to travel the whole system during a run. However, what we found to be of great importance is the number of realizations needed to obtain accurate results. At least 16 realizations of a lattice of 2^{10} sites is needed for the density-density correlation function to settle down to a consistent shape up to the second zero. Since the density-density correlation function is self-averaging, we have mostly worked with large systems of size 2^{16} which corresponds to 64 realizations of a system of size 2^{10} and we can safely neglect finite-size effects. A summary of the number and size of the simulations performed is given in Table II.

In Fig. 2 we plot $R(t)$ versus time on a logarithmic scale for the case $r = 5$ and $p = 0.25$. Two guiding lines of slopes $1/4$ and $1/3$, which have been suggested as possible asymptotic exponents, are included. Note that the case $\langle\rho\rangle = 1.1$ is equivalent to $\langle\rho\rangle = 0.9$ because of particle-hole duality. At best we see a gradual approach to an asymptotic power law. At late times the domain growth for $\langle\rho\rangle = 1.0$ seems to approach $1/3$, as suggested by the guiding lines. In contrast, for $\langle\rho\rangle = 0.4$ it is not possible to determine the asymptotic growth from comparison with the guidelines. In addition, there are slight differences (not fluctuations) between the data corresponding to $\langle\rho\rangle = 1.0$ and $\langle\rho\rangle = 0.4$ at early times. However, the general characteristics of the domain growth at least up to 10^6 time steps is independent of average overall density for $0.4 \leq \langle\rho\rangle \leq 1.0$.

There is not enough data in the asymptotic limit to fit to a simple power law; therefore, to account for the subleading asymptotics we fit to the form $R(t) = b + ct^a$. For $\langle\rho\rangle = \{1.0, 0.4\}$ a nonlinear curve fitting over

TABLE II. A summary of a representative set of simulations (Sim.) discussed in this paper. The size of the lattice (N), the maximum number of time steps (T), and the number of realizations (N_R) are listed for each choice of p and average density $\langle\rho\rangle$.

Sim.	p	$\langle\rho\rangle$	N	T	N_R
6a	0.25	1.0	2^{12}	2^{21}	8
6b	0.25	1.0	2^{14}	2^{20}	16
6c	0.25	1.0	2^{14}	2^{16}	64
6d	0.25	1.0	2^{10}	2^{16}	256
6g	0.25	1.0	2^{16}	2^{22}	1
6h	0.25	1.0	2^{14}	2^{25}	1
7a	0.25	0.4	2^{14}	2^{16}	80
7b	0.25	0.4	2^{16}	2^{21}	1
7d	0.25	0.4	2^{16}	2^{23}	1
7e	0.25	0.4	2^{16}	2^{20}	4
7f	0.25	0.4	2^{10}	2^{14}	512
7h	0.25	0.4	2^{14}	2^{24}	1
8a	0.01	1.0	2^{16}	2^{20}	1
8b	0.01	1.0	2^{10}	2^{17}	256
8c	0.01	0.4	2^{16}	2^{17}	4
9a	0.25	0.8	2^{16}	2^{22}	1
9b	0.25	1.1	2^{16}	2^{20}	4
9c	0.25	0.7	2^{16}	2^{20}	4

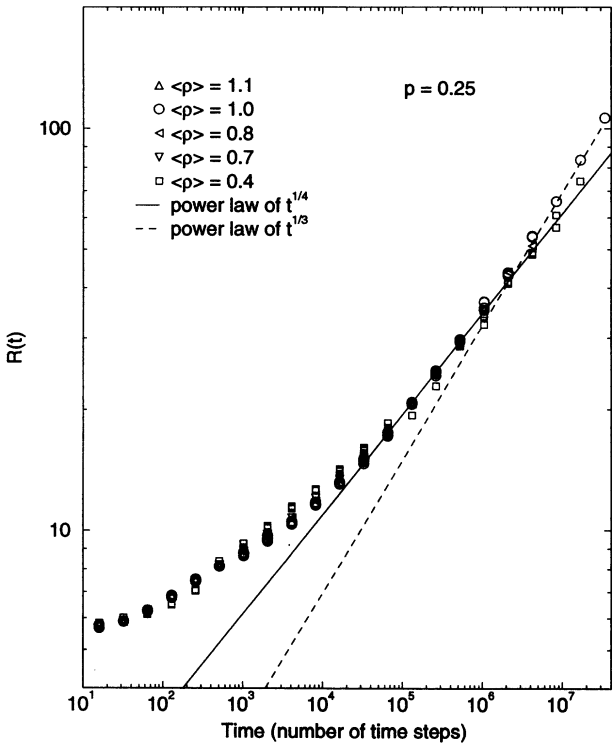

FIG. 2. The position of the first zero in $g(x,t)$, denoted by $R(t)$, is plotted against time on a logarithmic scale for several average densities. The solid and dashed lines are guidelines to indicate growth exponents of $1/4$ and $1/3$, respectively. The model parameters are for $r = 5$ and $p = 0.25$. The results are from all simulations except 8a, 8b, and 8c (see Table II).

times $t \geq 512$ gives an exponent of $a = \{0.349, 0.306\}$, respectively, which suggests that an asymptotic growth of $a = 1/4$ is too low an exponent. The form $R(t) = (b + ct)^a$ gives a poor fit because it does not yield a slow approach into the asymptotic regime. The local effective exponent $d \ln R(t)/d \ln t$ at our latest times is about $\{0.31, 0.29\}$ for $\langle\rho\rangle = \{1.0, 0.4\}$, respectively. If we pin the largest exponent to be $1/4$, no good fitting forms could be found. Thus the data are inconsistent with an asymptotic growth exponent of $1/4$. However, the data are consistent with an asymptotic exponent of $1/3$ which is predicted by a supplementary argument given below.

In Fig. 3 we show less extensive simulation results for the characteristic length scale in the case $r = 5$ and $p = 0.01$. The domain growth is extremely rapid at early times as is expected from the linear analysis of the lattice Boltzmann equation. Particles (holes) are attracted to one another very strongly, and at short length scales they have a ballistic type of motion. Therefore, particles (holes) within local neighborhoods rapidly form packed domains with virtually no minorities. At low densities particles need to travel some distance to find these local packets so the growth is not as rapid as with the half filled lattice. Once well defined domains have formed (after $t \approx 1000$ steps), the evaporation and condensation mechanism applies. Since the rate of evaporation is extremely low, it will *initially* control the domain growth. Logarithmic growth may occur at later times because there are only very weak density fluctuations, but there is no hope to unambiguously determine a power law or a logarithmic growth from simulation for $p \ll p_c$.

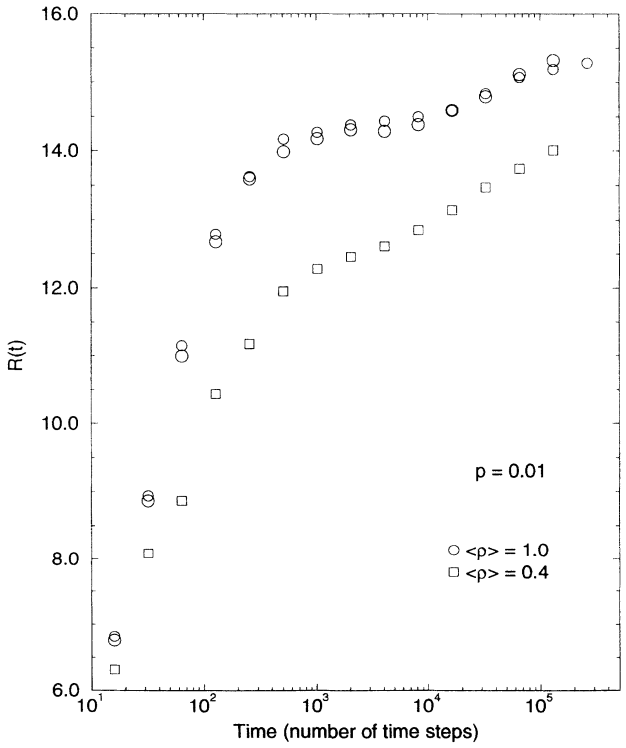

FIG. 3. The position of the first zero $R(t)$ of the function $g(x,t)$ is plotted against time on a semilogarithmic scale for the average densities of $\langle\rho\rangle = 1.0$ and $\langle\rho\rangle = 0.4$ with $r = 5$ and $p = 0.01$. The data are from simulations 8a, 8b, and 8c.

We give a supporting argument for an asymptotic domain growth law of $1/3$ by viewing the evaporation and condensation process according to the following picture. Consider a stochastic process in which there are many random walkers of types P and H "running a race." The P and H random walkers are placed on parallel tracks (one walker per track) in an alternating fashion so that every H walker has two neighboring P walkers and vice versa. The distance from the origin to a P and H walker represents the width of a high- and low-density domain, respectively. The random walkers are thus confined to the positive real axis. When a walker reaches the origin it is killed, and its two neighboring walkers, at distances l_1 and l_2, fuse to form a single walker at a distance $l = l_1 + l_2$.

There are *next*-nearest-neighbor-interactions between walkers to satisfy mass conservation. A P walker can increase its distance from the origin by one unit only if one of the P walkers on either side decreases its distance by one unit. The same applies to the H walkers. This interaction is implemented by assigning a random variable β_i to the ith walker which can take on the three possible values of -1, 0, or 1 with probabilities $p_i/2$, $1 - p_i$, and $p_i/2$, respectively. If $\beta_i = -1$, the $(i-1)$th walker steps $+1$ unit and the $(i+1)$th walker steps -1 unit. If $\beta_i = +1$, then just the reverse situation occurs, and if $\beta_i = 0$ nothing happens. Therefore, some walkers get farther away from the origin at the expense of other walkers getting closer and possibly dying. The number of walkers continuously decreases because we do not allow for the possibility of walkers to be created spontaneously. The characteristic length scale $L(t)$ is defined by the total length of the system $L_0 = \sum l_i$, divided by the number of domains.

For the moment, we consider the above stochastic process with $p_i = 1$ for all walkers. Then the growth rate can be found in terms of the time variable τ, which is the average number of *nonzero* random events per walker. The total number of domains $n(\tau)$ can be expressed as a summation over the distribution of walkers such that

$$n(\tau) = \frac{1}{2}\sum_{l=1}^{\infty} n_w(l,\tau) \,, \tag{13}$$

where $n_w(l,\tau)$ is the number of walkers (P and H) l distance away from the origin at time τ. The factor of $1/2$ is needed to prevent double counting. The rate of change of the number of domains is given by

$$\frac{d}{d\tau} n(\tau) = -\frac{1}{4} n_w(1,\tau) \,, \tag{14}$$

where a second factor of $1/2$ comes in as the probability that a walker one unit away from the origin will be absorbed at the origin. Making the scaling assumption that $n_w(l,\tau) = \tau^{-b}\tilde{n}_w(l/L(\tau))$ we then can Taylor expand Eq. (14) to yield

$$\begin{aligned} \frac{d}{d\tau} n(\tau) &= -\frac{\tau^{-b}}{4}\tilde{n}_w(1/L) \\ &= -\frac{\tau^{-b}}{4}\left[\tilde{n}_w(0) + \frac{1}{L}\tilde{n}_w'(0) + \cdots\right] , \end{aligned} \tag{15}$$

where $\tilde{n}_w(0) = 0$. Using the scaling form for n_w in Eq. (13) it is found that $n(\tau) = \tau^{-b} L(\tau) C_0$ with $C_0 = \frac{1}{2}\int_0^\infty \tilde{n}_w(z)\, dz$. From the fact that $L(\tau) = L_0/n(\tau)$ we note that $L^2 \sim \frac{L_0}{C_0}\tau^b$, which allows us to express Eq. (15) as

$$-\frac{1}{n}\frac{d}{d\tau}n = \frac{1}{L}\frac{d}{d\tau}L = \frac{\tilde{n}_w'(0)}{4C_0L^2} + O(1/L^3) \quad . \tag{16}$$

To leading order, we integrate Eq. (16) to obtain the asymptotic growth law $L(\tau) = A\tau^{1/2}$ (implying $b = 1$), where A will be a function dependent on the reduced density f_0. Not surprisingly, the scaling is of Gaussian type.

The above scaling analysis can be extended to obtain the functional form of the amplitude on the reduced density. The procedure follows in the same way as above, so we only sketch the main points. We make the natural assumption that the P and H walkers *separately* scale with the same scaling function (apart from a normalization constant) in terms of the average high-density domain length $f_0 L(\tau)$ and the average low-density domain length $\bar{f}_0 L(\tau)$, respectively. As a consequence of having $n(\tau) = n_P(\tau) = n_H(\tau)$, the distribution functions scale according to

$$\begin{aligned} n_P(l,\tau) &= n_0 \tau^{-b} F[l/f_0 L(\tau)]/f_0 \,, \\ n_H(l,\tau) &= n_0 \tau^{-b} F[l/\bar{f}_0 L(\tau)]/\bar{f}_0 \,, \end{aligned} \tag{17}$$

where n_0 is the number of domains initially and $F(z)$ is a scaling function with normalization $\int_0^\infty F(z)\, dz = 1$ and $F(0) = 0$. Using the relation $n_w(l,\tau) = n_P(l,\tau) + n_H(l,\tau)$ we find that $A = \sqrt{B(f_0^2 + \bar{f}_0^2)}/f_0\bar{f}_0$, where $B = F'(0)/2$. From simulation of the above stochastic model for the walkers, we have verified our scaling assumptions, the prediction for the asymptotic power law $L(\tau) = A\tau^{1/2}$, and the density dependence of the amplitude A, where the constant $B \approx 5$ was determined.

The quantity τ is related to the time t of the full evaporation-condensation process by

$$d\tau = \langle p_i \rangle dt \,, \tag{18}$$

where p_i corresponds to the probability per time step that a minority carrier successfully crosses the domain length l_i. It is more correct to speak about a *probability current* representing the flow of minority carriers from one parent domain (a source) to the other parent domain (a sink). Assuming a quasistationary flow, it is well known that $p_i \propto 1/l_i$. Using the differential form of the growth law in terms of τ, it follows that $L\, dL = A^2/2\, d\tau$, and taking $\langle p_i \rangle = C/L$ in Eq. (18) we obtain $L(t)^3 = 3CA^2 t/2$, which gives us the $1/3$ asymptotic growth law. This power law, with exponent of $1/3$, has also been verified by simulation when $p_i = p(l_i) = p(1)/l_i$ is used in the stochastic model. The results differ from the real simulation data in that the $1/3$ power law is almost immediately obtained.

The slow approach to the asymptotic regime in the real simulation data can be accounted for by realizing that domains of length $l \leq 2r$ must be treated differently from larger domains. If a domain width is less than $2r$ the rates of evaporation and condensation of carriers will respectively increase and decrease drastically. By choosing various forms for $p_i = p(l_i)$ for $l_i < 2r$, we have also been able to produce a slow approach to the asymptotic power law of $1/3$. Further work in this direction has been initiated. However, it is the average of $p(l_i)$ that is needed and if we assume that

$$\langle p_i \rangle = C_0/L + C_1/L^2 + C_2/L^3 + \cdots \,, \tag{19}$$

we obtain the same prediction as Huse [13] (not for the same reasons) for the asymptotic time dependence of the characteristic length scale. Therefore, we have fitted the $R(t)$ data plotted in Fig. 2 to the form

$$R(t) = A_0 t^{1/3} + A_1 + A_2 t^{-1/3} \tag{20}$$

for $\langle \rho \rangle = \{1.0, 0.4\}$. The resulting fits are excellent and for $t \geq 512$ we find $\{A_0 = 0.306, A_1 = 4.93, A_2 = 7.69\}$ at $\langle \rho \rangle = 1.0$ and at $\langle \rho \rangle = 0.4$ we find $\{A_0 = 0.256, A_1 = 8.31, A_2 = -17.2\}$. At present, the assumption that $\langle p_i \rangle$ may be expanded in powers of $1/L$ is only a suggestion. However, provided small domain sizes play an irrelevant role in the late stages of coarsening, this simple picture predicts the asymptotic growth to obey a $1/3$ power law.

There is nothing in the above argument which draws a distinction between the cases $p = 0.25$ and $p = 0.01$, which were compared in Figs. 2 and 3. The growth law at short times is more complicated for $p = 0.01$ than for $p = 0.25$ because the rate of evaporation is extremely low and the motion of the minority carriers gradually changes from ballistic to diffusive as a domain length increases. Nevertheless if one waited long enough, the domain growth will become diffusion controlled and an asymptotic growth exponent of $1/3$ will presumably appear. This regime is unreachable by simulation.

IV. DYNAMICAL SCALING

Given that well defined domains form and grow, we now address the question of whether dynamical scaling [9] holds. If dynamical scaling holds, then the entire time dependence of the equal time density-density correlation function enters implicitly through the single characteristic length scale of the system, so $g(x,t) = \tilde{g}[x/R(t)]$ at long times. Equivalently dynamical scaling in the structure function predicts $S(k,t) = R(t)\tilde{S}[kR(t)]$ for one dimension. Since the approach to the asymptotic growth law is so slow, it is possible (even expected) that no scaling will be observed. The $r = 5$ and $p = 0.01$ data cannot be considered because it is certainly not in the scaling regime although the growth is so slow that $g(x,t)$ and $S(k,t)$ barely changed over the period $10^3 < t < 10^6$.

First we look at the density-density correlation function $g(x,t)$ for the data at a half filled lattice with $r = 5$ and $p = 0.25$. In Fig. 4 we plot $g(x,t)$ against the scaled variable z, given as $z = x/R(t)$, for data with times 2^9 to 2^{21} (i.e., a span of ~ 3.6 decades). Unlike the kinetic Ising models $g(0,t)$ is, in general, not equal to one because each node may have 0, 1, or 2 particles. At early

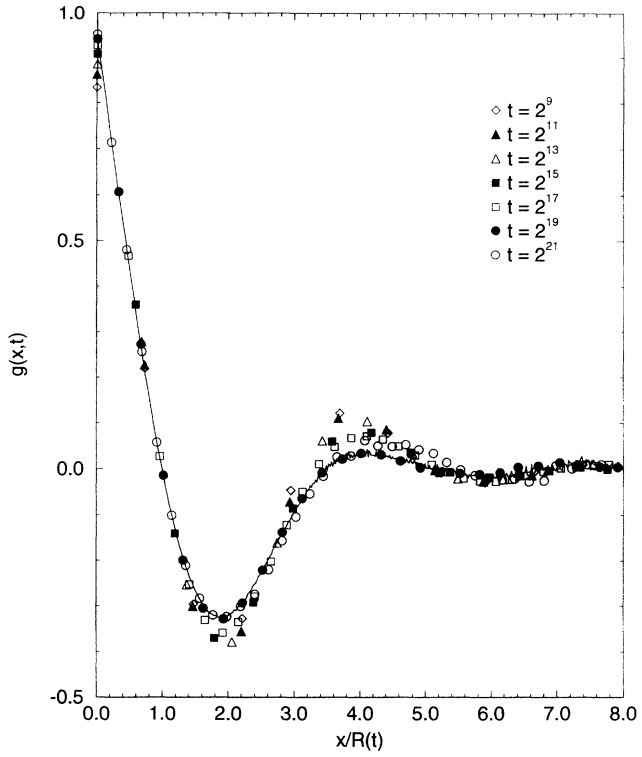

FIG. 4. A plot of $g(x,t)$ for a variety of times, against the scaled variable $z = x/R(t)$. The data come from simulation 6 with $r = 5$, $p = 0.25$, and $\langle\rho\rangle = 1.0$. The number of realizations that are averaged varies for different times. As defined in the text, the total number of effective realizations for times from 2^9 to 2^{15} is 103, from 2^{17} to 2^{19} it is 23, and for 2^{21} it is 7. The solid line represents an average over all times $t \geq 2^{20}$ corresponding to 38 effective realizations.

times $g(0,t) < g(0,\infty)$ because many interfaces of finite width are present in the system. The value of $g(0,t)$ at long times will approach a constant less than unity because the average density of the two phases will be ρ_m and $2 - \rho_m$, where ρ_m is the average minority carrier density. An estimate of the minority density is given by

$$\rho_m \approx 1 - \sqrt{g(0,\infty) + (\langle\rho\rangle - 1)^2}\,, \tag{21}$$

which was obtained by assuming infinitely sharp interfaces between domains of a uniform, mean density. Noting from the data that $g(0,\infty) \approx 0.97$ or slightly greater, it is found that $\rho_m \approx 0.015$ or less.

The data points plotted in Fig. 4 are from the combined collection of simulation no. 6 listed in Table II at $\langle\rho\rangle = 1.0$ for each relevant time. We first averaged over all the correlation functions at a particular time with a relative weight of $N_R N/2^{14}$, which corresponds to the effective number of realizations on a lattice of size 2^{14} sites. Here N_R is the number of realizations and N the system size. After this averaging, the position of the first zero $R(t)$ is found and then the functions are scaled. For example, the data corresponding to $t = 2^9$ have a total of 103 effective realizations whereas that for $t = 2^{21}$ only has seven. The solid line in Fig. 4 was obtained by first scaling the resulting correlation function for each data set of simulation no. 6 for times $2^{20} \leq t \leq 2^{25}$ and then averaging over all the scaled functions with the appropriate weight.

Clearly the data of Fig. 4 is not collapsing onto a single curve, at least for data with $t \leq 2^{17}$. With the exception of the first few data points the method we use to scale $g(x,t)$ will cause the curves to trivially collapse onto themselves for $0 \leq x/R(t) \leq 1$. Considering the wide range of time, however, dynamical scaling is holding approximately even in the time regime before domain growth reaches a power-law form. We expect that dynamical scaling will hold once the asymptotic domain growth is reached. From Fig. 2 we see a power-law growth is just setting in after $t = 2^{20} \approx 10^6$ time steps. Provided that $t = 2^{20}$ is indeed the start of the scaling regime, an average over all the data for $t \geq 2^{20}$ should represent the scaling function as shown in Fig. 4 by the solid line. It is essential to use as many realizations as we have available since fluctuations mask the results as can be seen by comparing the $t = 2^{21}$ data set with the solid line. A good indication that the solid line represents the scaling function $\tilde{g}(z)$ is that the $t = 2^{19}$ data set coincides with the curve well.

In Fig. 5 we plot the scaled structure factor $S(k,t)/R(t)$ versus the scaled wave number $kR(t)$ for the same range of times as in Fig. 4. The averaging weights for the structure factors are the same as for the correlation functions of Fig. 4. We first scaled the structure

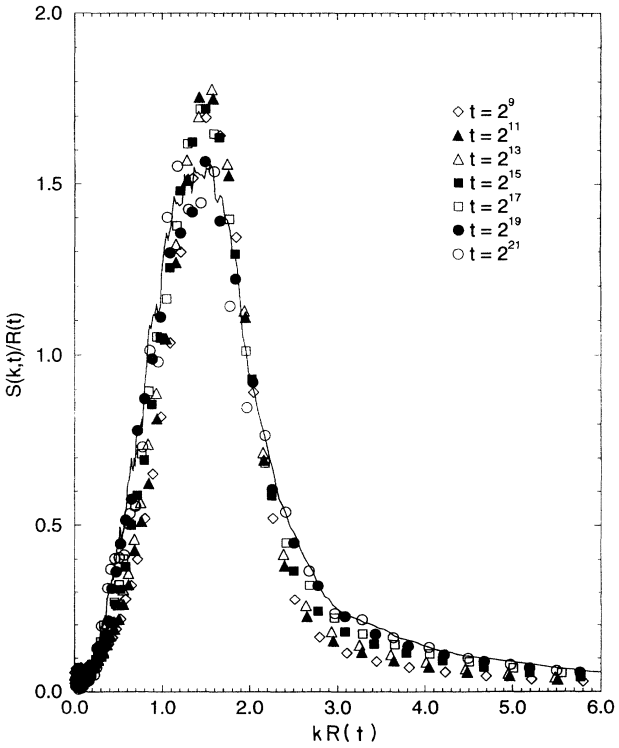

FIG. 5. A plot of the scaled structure factor $S(k,t)/R(t)$ against $kR(t)$ is given for various times with $r = 5$, $p = 0.25$, and $\langle\rho\rangle = 1.0$. The data used are the same as those used in Fig. 4. The solid line represents an average over all realizations with $t \geq 2^{20}$.

factor of each data set using the $R(t)$ that was used in scaling the correlation functions. These scaled structure factors were then averaged. The solid line was obtained by averaging over all the scaled structure factors with $t \geq 2^{20}$.

The data collapse is remarkably good, although we see again that scaling is only approximately holding. The peak gradually decreases as the structure factor broadens until it reaches a limiting scaling form which is believed to be well represented by the solid line shown. The discrepancy of the data collapse near the peak of the structure function is commonly observed in experiments [14] and could be contributed to corrections to scaling before the true asymptotic behavior is reached. The results for the scaled structure factor in Fig. 5 using $R(t)$ as a scaling variable demonstrates that the first zero in the density-density correlation function is an excellent way of defining the characteristic length scale of the system.

The density-density correlation functions obtained from simulation no. 7 with $r = 5$, $p = 0.25$, and $\langle \rho \rangle = 0.4$ are plotted in Fig. 6 against, $z = x/R(t)$, over the time range $2^9 - 2^{21}$. The scaled correlation functions at each time were obtained in the same way as described above for the half filled lattice. The solid line is an average over all the data sets shown and is virtually identical to an average over all data sets for $t \geq 2^{20}$. An initial growth in $g(0,t)$ is again seen, and with the estimate of $g(0,\infty) \approx 0.61$ it follows from Eq. (21) that $\rho_m \approx 0.015$ or less. Since ρ_m is the same for the 1/2 and 1/5 filled lattice, the idea that a domain of length $l > 2r$ will have a constant minority carrier density is confirmed.

With the exception of the earliest time of $t = 2^9$, the data collapse in Fig. 6 indicates the density-density correlation function scales. This scaling is actually surprising because if the asymptotic power law is $t^{1/3}$, as argued previously, then from Fig. 2 it is seen that neither has the asymptotic regime been reached nor is there any indication of a cross over. If only *one* scaling regime exists, then as the evaporation and condensation mechanism applies equally well at all average densities, we cannot presently explain why scaling is observed prior to an asymptotic power-law growth. If, however, small domains play a relevant role in determining the asymptotic growth law, then one would expect an effective exponent dependent on the average density. This possible explanation is consistent with there being a single scaling regime.

The scaling forms for $\tilde{g}(z)$ at 1/2 and 1/5 filled lattice are considerably different, and the scaled correlation functions for $\langle \rho \rangle = \{0.9, 0.8, 0.7\}$ gradually flatten and become shallower as they shift (not linearly) from the form given in Fig. 4 to that of Fig. 6. These correlation functions cannot be simply related by an additional scaling factor dependent on average density [9] because the functional form changes.

In Fig. 7 we present a log-log plot of the corresponding scaled structure factor $S(k,t)/R(t)$ against the scaled

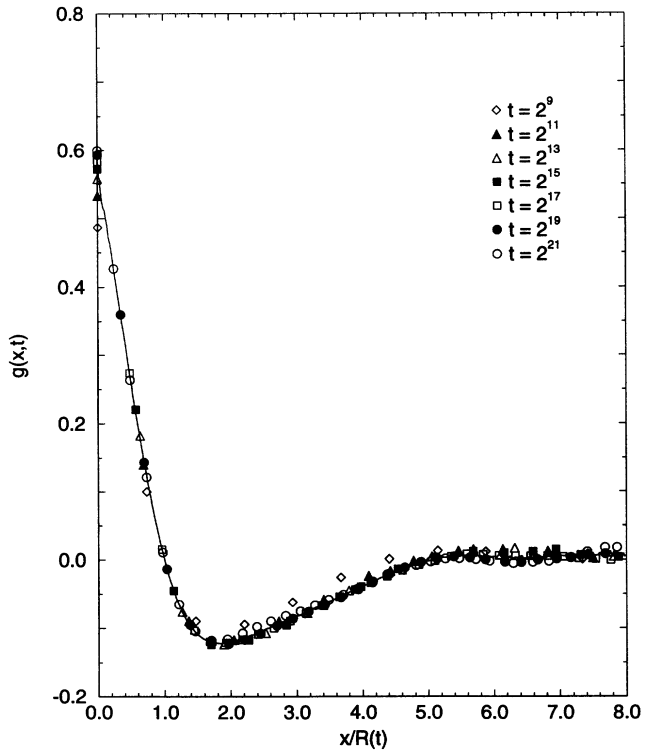

FIG. 6. A plot of $g(x,t)$ against the scaled variable $x/R(t)$ is given for various times for simulation 7 with $r = 5$, $p = 0.25$, and $\langle \rho \rangle = 0.4$. The number of realizations that have been averaged varies for different times. As defined in the text, the total number of effective realizations for times from 2^9 to 2^{13} is 137, for 2^{15} it is 105, from 2^{17} to 2^{19} it is 25, and for 2^{21} it is 9. The solid line is an average over all the data sets shown except for $t = 2^9$.

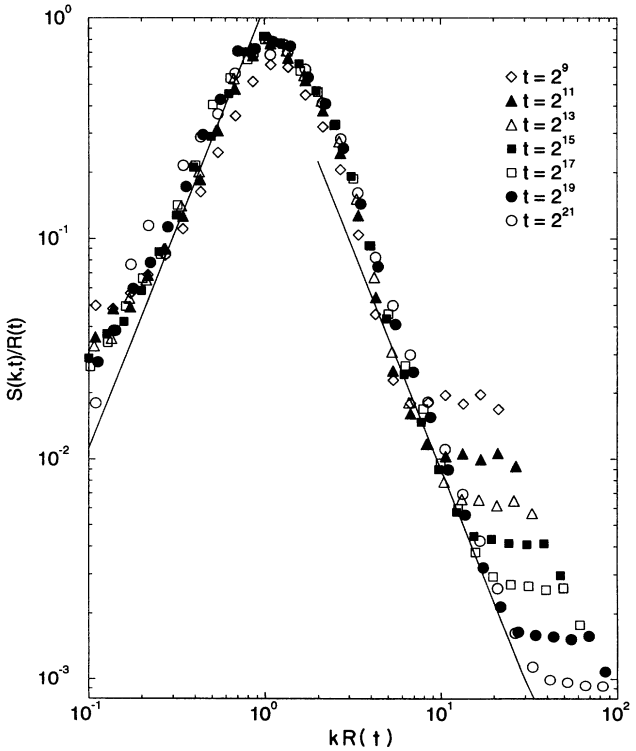

FIG. 7. A plot on a logarithmic scale of the scaled structure factor $S(k,t)/R(t)$ against the scaled wave number $kR(t)$ is given for various times with $r = 5$, $p = 0.25$, and $\langle \rho \rangle = 0.4$. The data used here are the same as used in Fig. 6. The solid lines are included as guidelines having slopes of ± 2.

wave number $kR(t)$. The left guideline in Fig. 7 has a slope of $+2$, which suggest that $S(k,t) \sim k^2$ for small wave numbers. A quadratic dependence on k for $kR(t) < 1$ is a consequence of mass conservation [9]. The deviation from this power law for $kR(t) \ll 1$ may be caused by the transient decay of the initial condition where $S(k,0) \approx S_0$ for all $k \neq 0$.

The right guideline of Fig. 7 has a slope of -2. The structure factor is seen to fall off in agreement with Porod's law [9], which predicts that for a conserved, scalar order parameter $S(k,t) \sim k^{-d-1}$ for $kR(t) \gg 1$. The wings that level out at successively larger values of $kR(t)$ are a consequence of the discrete nature of the model. The transition point where the structure factor levels out occurs at a *constant* wave number corresponding to approximately the inverse of a length of seven lattice constants. This indicates that on this and smaller length scales the discreteness of the microscopic dynamics makes the system too noisy to resolve. We note that the same small and large wave number dependence is observed for the structure factors calculated for a half filled lattice.

V. DISCUSSION

In this paper, we have introduced a diffusive lattice gas to model a one-dimensional system of particles with an attractive interaction over a length r. For sufficiently large r, the system phase separates into well defined domains. Driven by fluctuations, the system coarsens toward a phase-separated state. However, fluctuations may ultimately destroy the fully phase separated state by breaking the system up into large domains having some typical coherence length ξ. Presumably $\xi \gg 2^{16}$ for the parameters considered here.

The ripening process is caused by the evaporation and condensation of carriers diffusing between parent domains. Based on a simple picture for the evaporation and condensation mechanism, which is independent of the microscopic details of the model, we have argued that the domain growth law will asymptotically approach $t^{1/3}$. The simulation data for the domain growth are consistent with the conjecture that $R(t) = A_0 t^{1/3} + A_1 + A_2 t^{-1/3} + \cdots$ where the coefficients are dependent on average density and other model parameters. We have done a few simulation runs (for checking purposes) on a model where the interaction is determined by the difference in total occupation number at the nodes $x \pm r$. We find similar results as those for the much simpler model described in this paper. Therefore we suspect that the observed properties that have been discussed are universal in character and not model dependent.

The observation of scaling of the density-density correlation function and structure factor for a $1/5$ filled lattice *before* an asymptotic growth law of $t^{1/3}$ had set in leaves open the possibility that an effective asymptotic exponent is present which depends on average density. Further study of the simplified growth model described in Sec. III has been initiated to determine whether such an effective exponent exists and to study the distribution in domain sizes.

ACKNOWLEDGMENTS

We would like to thank M.H. Ernst for many valuable suggestions. One of us (D.J.J.) would like to thank H. van Beijeren and R. Dickman for helpful comments and is supported by the Stichting voor Fundamenteel Onderzoek der Materie. A.J.M. would like to thank A. Bray for much helpful advice.

[1] U. Frisch, B. Hasslacher, and Y. Pomeau, Phys. Rev. Lett. **56**, 1505 (1986); U. Frisch, D. d'Humieres, B. Hasslacher, P. Lallemand, Y. Pomeau, and J.P. Rivet, Complex Syst. **1**, 648 (1987).

[2] B.M. Boghosian and C.D. Levermore, Complex Syst. **1**, 17 (1987).

[3] K. Hwang, B. Schmittmann, and R.K.P. Zia, Phys. Rev. Lett. **67**, 326 (1991).

[4] M. Hénon, J. Stat. Phys. **68**, 353 (1992); H.J. Bussemaker and M.H. Ernst, *ibid.* **68**, 431 (1992); Transp. Theory Stat. Phys. **23**, 147 (1994).

[5] D.H. Rothman and J.M. Keller, J. Stat. Phys. **52**, 1119 (1988); C. Appert and S. Zaleski, Phys. Rev. Lett. **64**, 1 (1990); F.J. Alexander, I. Edrei, P.L. Garrido, and J.L. Lebowitz, J. Stat. Phys. **68**, 497 (1992); M. Gerits, M.H. Ernst, and D. Frenkel, Phys. Rev. E **48**, 988 (1993).

[6] A.B. Bortz, M.H. Kalos, J.L. Lebowitz, and M.A. Zendejas, Phys. Rev. B **10**, 535 (1974); J.G. Amar, F.E. Sullivan, and R.D. Mountain, *ibid.* **37**, 196 (1988).

[7] T.M. Rogers, K.R. Elder, and R.C. Desai, Phys. Rev. B **37**, 9638 (1988); E.T. Gawlinski, J. Vinals, and J.D. Gunton, *ibid.* **39**, 7266 (1989).

[8] M.H. Ernst, in *Liquids, Freezing and Glass Transition,* Proceedings of the Les Houches Summer School of Theoretical Physics, Les Houches, 1989, edited by J.P. Hansen, D. Levesque, and J. Zinn-Justin (Elsevier Science Publishers B.V., Amsterdam, 1991), Session L1, p. 45.

[9] H. Furukawa, Adv. Phys. **34**, 703 (1985).

[10] K. Binder and D. Stauffer, Phys. Rev. Lett. **33**, 1006 (1974).

[11] T. Gobron, J. Stat. Phys. **69**, 995 (1992).

[12] W.H. Press, B.P. Flannery, S.A. Teukolsky, and W.T. Vetterling, *Numerical Recipes* (Cambridge University Press, Cambridge, 1989).

[13] D.A. Huse, Phys. Rev. B **34**, 7845 (1986).

[14] S. Komura, Phase Transitions **12**, 3 (1988).